Application of Image Analysis for Characterization of Spatial Arrangements of Features in Microstructure

PASCAL LOUIS and ARUN M. GOKHALE

A number of microstructural processes are sensitive to the spatial arrangements of features in microstructure. However, very little attention has been given in the past to the experimental measurements of the descriptors of microstructural distance distributions due to the lack of practically feasible methods. We present a digital image analysis procedure to estimate the microstructural distance distributions. The application of the technique is demonstrated *via* estimation of K function, radial distribution function, and nearest-neighbor distribution function of hollow spherical carbon particulates in a polymer matrix composite, observed in a metallographic section.

I. INTRODUCTION

SPATIAL arrangements of features in a microstructure can be quantified in terms of the distances between the corresponding features. Distribution of distances between features in a microstructure is an important microstructural attribute. The microstructural distance distributions affect the microstructural processes that involve short range, and/or long-range particle-particle interactions (or feature to feature interactions, in general). For example, diverse phenomena, such as formation and growth of microcracks during thermal cycling of metal matrix composites,[1,2] damage accumulation and fracture behavior of composites,[3,4] particle coarsening,[5,6] liquid-phase sintering,[8,9] microstructural evolution during solid-state transformations where nucleation occurs on the second-phase particles,[10,11] microvoid induced ductile fracture processes in metals and alloys,[12,13] creep cavitation,[14] and creep crack growth,[15] crucially depend on the distances between the relevant microstructural features.

The microstructural distance distributions may be significantly altered when a material is processed in reduced gravity or microgravity, particularly if a liquid phase is involved. In such a case, it is desirable to quantify the changes in the microstructural distance distributions due to reduced gravity and to quantify and model the role of gravity in the microstructural evolution processes.

Very few investigations deal with the quantitative effect of the spatial distribution of microstructural features on the physical/mechanical properties of materials or on the microstructural evolution during materials processing. An important reason for this is the lack of well-developed practical techniques to quantify the spatial distribution of microstructural features and, as a result, the lack of realistic and flexible quantitative models to represent the spatial distribution in the computer simulation or analytical theoretical studies.

PASCAL LOUIS, Research Engineer, is with Aerospatiale, Centre Commun de Recherches, 92152 SURESNES Cedex, France. ARUN M. GOKHALE, Professor, is with the School of Materials Science and Engineering, Georgia Institute of Technology, Atlanta, GA 30332-0245.

Manuscript submitted September 2, 1994.

It is the purpose of this article to present an image analysis procedure to obtain the basic experimental data necessary to quantify the spatial arrangement of microstructural features in metallographic sections. To characterize spatial distributions, the necessary basic data consist of centroid coordinates and sizes of the microstructural features of interest. These raw data can be processed to compute the descriptors of spatial order, such as nearest-neighbor distribution,[16,17,18] radial distribution,[19-22] K function,[19-22] pair-correlation function,[21,22,23] or parameters such as short range and long range microstructural gradients.[24] An image analysis procedure was developed to automatically extract centroid coordinates (and feature size, *etc.*) of the microstructural features observed on *different* fields of view and referred to the same origin: this is essential to compute the distances between the particles that may not be in the same field of view. The image analysis algorithm provides a practical procedure to acquire the centroid coordinates data of thousands of particles to quantify the short-range as well as long-range affinity (or lack of it) among the features. A simple computer program utilizes these raw data to compute the descriptors of spatial distribution, such as nearest-neighbor distribution and radial distribution.

For population of spherical particles, stereological relationships are available to estimate the three-dimensional (3-D) radial distribution from the corresponding experimentally measured two-dimensional (2-D) radial distribution of the particle sections observed in a metallographic plane.[19,21,23] In the case of composites having continuous aligned fibers, the spatial distance distributions of fiber centers observed in a metallographic plane perpendicular to the fibers are sufficient for the characterization of the spatial distribution of the fibers and hence no stereology is necessary in such cases.

In the present study, the image analysis procedure is applied to quantify the spatial distribution of hollow spherical carbon particles in a polymer matrix composite. The measurements are performed on two specimens having different volume fractions of particulates but the same size frequency function. A brief background on microstructural distance distributions is presented in

Section II. The image analysis procedure and practical example are given in Sections III and IV.

II. DESCRIPTORS OF MICROSTRUCTURAL DISTANCE DISTRIBUTIONS

Let N_v be the *average* number of particle or feature centroids per unit volume of microstructure. Focus on one particle whose centroid is at location (X_i, Y_i, Z_i) in the microstructural space. Draw a test sphere of radius R around this particle (*i.e.*, having the center at (X_i, Y_i, Z_i)). Let $K'(R)$ be the total number of other particle centroids contained in the test sphere. Obviously, the quantity $K'(R)$ depends on the location of the test sphere (*i.e.*, (X_i, Y_i, Z_i)), the distance R, and the spatial arrangement of the particle centroids in the microstructure. An average value, $K(R)$, can be obtained by averaging $K'(R)$ over all the particle centroid locations (X_i, Y_i, Z_i) in the microstructural space. The function $K(R)$ is called the K function,[19-23] and it gives the average number of particles (strictly speaking, particle centroids) in a sphere of radius R drawn around the centroid of an arbitrary particle or feature of interest in the microstructure. For a collection of randomly distributed particles, $K(R)$ is equal to $(4\pi R^3/3) \cdot N_v$; a value higher than this signifies clustering, and a lower one indicates repulsion.

The radial distribution function $G(R)$ is an alternate descriptor of the spatial arrangement of particle (or feature) centroids. It is defined as follows:[19,20,21]

$$G(R) = \frac{1}{(4\pi R^2 \cdot N_v)} \cdot \left\{\frac{dK(R)}{dR}\right\} \qquad [1]$$

The quantity $(4\pi R^2 \cdot N_v \cdot dR) \cdot G(R)$ is equal to the average number of particle centroids in a spherical shell of radii R and $(R + dR)$ around an arbitrary particle. For a random spatial distribution of the particles, $G(R)$ does not depend on R and it is equal to 1. For a clustered distribution of particle centroids, $G(R)$ is greater than 1 for small values of R. It is composed of a combination of delta functions for an ordered array of particles.

Note that the radial distribution function is related to the derivative of the K function (Eq. [1]), and hence it is more sensitive to changes in the spatial order than is the K function. The radial distribution function is particularly useful to quantify short-range particle-particle interactions. For most of the spatial arrangements of particles, $G(R)$ approaches 1 for a sufficiently large value of R, and it approaches zero as R tends to 0.

The radial distribution function contains information concerning the spatial arrangement of particle centers, but it gives no information concerning correlations between sizes and relative locations of the particles. For example, it does not tell us if the small particles are preferentially located near the larger particles, and so on. The pair correlation function contains such information. It is defined as follows:[21,22,23]

$$C(\Gamma_1, \Gamma_2, R) = \left\{\frac{1}{4\pi R^2 \cdot n_v(\Gamma_2)}\right\} \cdot \left\{\frac{d^2Q(\Gamma_1, \Gamma_2, R)}{d\Gamma_2 \cdot dR}\right\} \qquad [2]$$

$n_v(\Gamma_2)$ is the particle size distribution function, such that $n_v(\Gamma_2) \cdot d\Gamma_2$ is the number of particles in the size range Γ_2 to $(\Gamma_2 + d\Gamma_2)$ per unit volume of microstructure. The value of $Q(\Gamma_1, \Gamma_2, R)$ is the *average* number of particle centroids belonging only to the particles of size *smaller* Γ_2 in a sphere of radius R centered on a particle of size Γ_1. The value of $C(\Gamma_1, \Gamma_2, R)$ is the pair correlation function for the particles of the sizes Γ_1 and Γ_2 separated by distance R. The pair correlation function is 0 for $R \leq (\Gamma_1 + \Gamma_2)$, and it approaches 1 as R tends to infinity. For a random spatial distribution of particle centroids and uncorrelated particle sizes, the value of the pair correlation function is equal to 1 for all the values of R, Γ_1, and Γ_2. The pair correlation function is particularly useful in the study of processes, such as particle coarsening, where small particles may be preferentially located near the larger ones.[5,6]

In the deformation and fracture processes, such as ductile fracture and[12,13] creep crack growth and fracture,[15] the nearest-neighbor distribution function and average nearest-neighbor distance are the relevant microstructural parameters. The nearest-neighbor distribution function[16,17,18] is described by the probability density function $P(R)$, such that $P(R) \cdot dR$ is equal to the probability that there is no other particle centroid in a sphere of radius R around a given particle *and* there is at least one particle centroid in the spherical shell of radii R and $(R + dR)$. The average nearest-neighbor distance $\bar{R}$ is given by the following equation:

$$\bar{R} = \int_0^\infty R \cdot P(R) \cdot dR \qquad [3]$$

For randomly distributed point particles, $\bar{R}$ is equal to $0.554 \cdot (N_v)^{-0.333}$. In a manner similar to the nearest-neighbor distribution function, one can define 2nd, 3rd, . . . nth nearest-neighbor distributions.[22]

The materials microstructures are usually characterized from observations on representative 2-D metallographic sections through the 3-D microstructural space of interest. Thus, the basic microstructural data often pertain to the 2-D metallographic sections. All the preceding descriptors of distance distributions can be analogously defined for the 2-D microstructural sections. The K function pertaining to 2-D microstructural section, $k(r)$ is defined as the average number of particle *section* centroids in a *circle* of radius r, centered on an arbitrary particle section. The radial distribution function $g(r)$ pertaining to a 2-D microstructural section is defined as follows:

$$g(r) = \left\{\frac{1}{2 \cdot \pi \cdot r \cdot N_A}\right\} \cdot \left\{\frac{dK(r)}{dr}\right\} \qquad [4]$$

where N_A is the average number of particle section centroids per unit area of the metallographic section. Note that the lower-case symbols denote the distance distributions in the 2-D sections. The nearest-neighbor distribution function in a 2-D section is described by the probability density function $p(r)$, such that $p(r) \cdot dr$ is the probability that there is no other particle section centroid in a circle of radius r centered on an arbitrary particle section of interest *and* there is at least one particle section centroid in the circular ring of radii r and $(r + dr)$.

The pair correlation function for 2-D microstructural section $c(\tau_1, \tau_2, r)$ can be defined as follows:

$$c(\tau_1, \tau_2, r) = \left\{\frac{1}{2 \cdot \pi \cdot n_a(\tau_2)}\right\} \cdot \left\{\frac{d^2 q(\tau_1, \tau_2, r)}{dr d\tau_2}\right\} \quad [5]$$

$n_A(\tau_2)$ is the particle-section size distribution observed in the metallographic section. The value of $q(\tau_1, \tau_2, r)$ is the average number of particle-section centers belonging only to the particle sections smaller than τ_2 in a circle of radius r centered on an arbitrary particle section of size τ_1.

If microstructural distance distributions are experimentally measured on representative 2-D metallographic sections, then under certain conditions, the corresponding *3-D* distance distributions can be estimated by using stereological relationships.[19,21,23] For example, if the particle shape can be assumed to be spherical, then the 3-D radial distribution function $G(R)$ and the corresponding 2-D function $g(r)$ measured on a metallographic section are related through the following stereological equation:[19]

$$g(r) = \left\{\frac{1}{4(\bar{\Gamma})^2}\right\} \cdot \int_0^\infty F(u) \cdot G[(r^2 + u^2)^{1/2}] \cdot du \quad [6]$$

where,

$$F(u) = 2 \cdot \int_0^\infty \left[1 - f\left\{\frac{u - v}{2}\right\}\right] \cdot \left[1 + f\left\{\frac{u + v}{2}\right\}\right] \cdot dv \quad [7]$$

where $\bar{\Gamma}^*$ is the average particle radius, and f is the cumulative size frequency function of the spheres. Note that in Eq. [6], the desired 3-D radial distribution function G is under the integral sign, and hence numerical solution to this integral equation is necessary for the estimation of G.

III. IMAGE ANALYSIS TECHNIQUE

To estimate any of the distance distributions in a 2-D metallographic section, it is necessary to measure the (X, Y) coordinates of the observed particle-section centers and the corresponding section sizes. To obtain statistically meaningful measures, it is essential to perform these measurements on a large number of particle sections distributed over many fields of view (or frames), and hence automatic digital image analysis is *essential*: for all practical purposes, these measurements cannot be performed manually. In the digital image analysis, the microstructural distances are measured in units of pixels; the absolute sizes are calculated from this information by using the calibration factor, which depends on the microscope magnification. The minimum distance that can be measured is 1 pixel. For estimation of the particle section sizes with a measurement error of less than 10 pct, measurements have to be carried out at a microscope magnification where the particle image sizes are of the order of 10 to 20 or more pixels, so that the measured sizes have an error of less than 1 pixel (*i.e.*, less than 10 pct). At such magnifications, for a number of important classes of microstructures, on the average about 10 to 50 particles are present in an image frame (field of view). Further, in most of the cases, microstructural distances up to about 5 to 10 times the mean free path (average uninterrupted surface to surface distance between the particles through the matrix) have to be measured to obtain meaningful distance-distribution data. Thus, it is necessary to measure the distances between the particles that may *not* be in the same image frame or field of view (Figure 1). To measure such distances, it is obviously necessary to know the distances between the different image frames on the metallographic plane with an error of less than few pixels. Alternately, a procedure must be developed to obtain the (X, Y) particle center coordinates of the particles in all the different image frames *referred to the same (0, 0) origin*; the distance between the centers of the particles situated in different image frames can be then computed by using simple distance formula of coordinate geometry. This approach is adopted in the present work. The limitation on the size of the image frame (typically 512 × 512 pixels) also creates another problem due to the associated "edge effect." It is necessary to properly account for the particles that are only partly in the image frame, and their centers may be outside the image frame. Ignoring the particles on the edges of the image frame may introduce a bias of unknown extent in the measured distance distribution functions. This bias due to edge effect can be eliminated for all the practical purposes if a large number of contiguous fields of view (say about 35 to 50) can be precisely "pasted" together by developing an appropriate image analysis software. In the present work, such software is developed for the VIDAS image analysis system supplied by Carl Zeiss, Inc. (Germany). However, the basic algorithm is applicable to any modern image analysis system. Once different contiguous image frames are pasted together, the distance between the consecutive frames is simply equal to length of the image frame (*i.e.*, 512 pixels in the present case), and hence the (X, Y) coordinates of the particle centers in the different image frames can be referred to the same

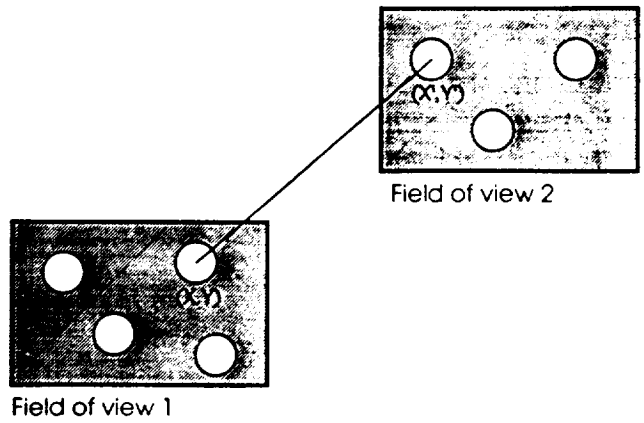

Fig. 1—Measurement of distances between particles located in different fields of view. Note that to calculate distance from (X, Y) to (X', Y'), it is necessary to have the same reference origin for both fields of view

(0, 0) origin by simple translation of the coordinates. The resulting coordinates and the respective particle sizes then form the basic raw data necessary to compute any distance distribution. The algorithm for the image analysis software to paste the image frames and to extract the (X, Y) center coordinates and the particle image size data is as follows.

The first image frame (field of view) is selected arbitrarily and stored in the memory of the image analyzing computer. The right border (having about a 50-pixel width) of this image is pasted on the left edge of the next approximately contiguous live-image frame (field of view), and the microscope stage is moved and adjusted so as to fit the right border of the previous frame to the left edge of the live image within about 10 to 20 pixels; this rough matching is done manually by the operator. At this point, the image of the live frame is grabbed and translated pixel by pixel until it perfectly matches with the right border of the previous field displayed on the screen.* Once a satisfactory match (within one pixel) is achieved, the second image frame is stored. The same procedure is continued with successive image frames. In this manner, a composite global frame of precisely contiguous 35 image fields (5 × 7 field of view) is stored in the computer; the upper limit on the number of image fields is set by the hard disk size and not by the image-analysis procedure. The successive image fields in the composite global frame are numbered in a serial order. The top left-hand corner of the first frame is designated as (0, 0) and is origin of the coordinate system (Figure 2).

*Note that the image can be translated by a preset number of pixels *via* a combination of commands available in the image analyzer.

Although the composite global image consisting of 35 fields of view is stored in the computer memory, the image analyzer can characterize only one image frame of the size 512 × 512 pixels at a time, and hence the creation of a composite global image by itself does not eliminate the edge effect. To solve this problem, a *measurement frame* of one-fourth of the size of 512 × 512 pixel frame is defined. The composite global image is divided into a number of such frames. For example, in Figure 3, the composite image of 16 fields of view is divided into 49 contiguous measurement frames. One-fourth of each of these stored image frames, containing the corresponding part of the measurement frame, is recalled on the analysis screen of the image analyzer; the measurement frame is at the center of the screen. Figure 4 shows this arrangement. In Figure 4, the dashed lines are the boundaries of the measurement frames; the measurements are performed on the measurement frame located in the center and completely inside the analysis screen. The measurements are performed only on those particles whose centroids are inside the measurement frame (for example, dark particles in Figure 4). The image analyzer gives (X', Y') centroid coordinates and particle sizes of these selected particles. At these stage, the centroid coordinates (X', Y') are with respect to the $(0', 0')$ origin at the bottom left-hand corner of the *measurement frame*, whose location with respect to the fixed origin (0, 0) of the composite global frame (Figure 2) is precisely known. Thus, (X, Y) centroid coordinates with respect to the fixed (0, 0) origin of the composite global frame can be calculated from local (X', Y') centroid coordinates by simple coordinate translation. The (X, Y) centroid coordinates and corresponding particle sizes are stored in a file as a series of triplets

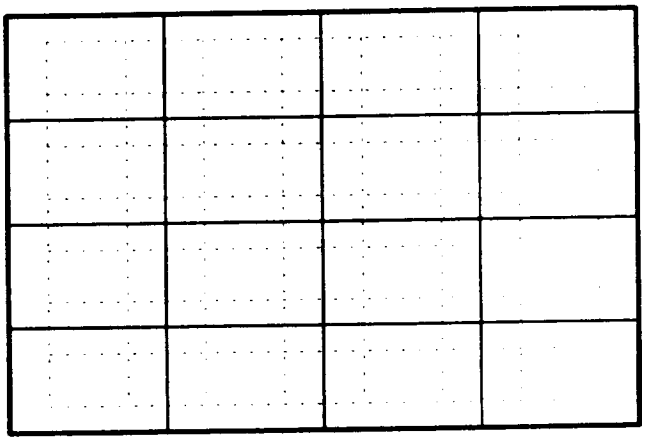

Fig. 3—Division of composite global image frame made up of 16 contiguous fields of view (solid lines) into a set of measurement frames (dashed lines).

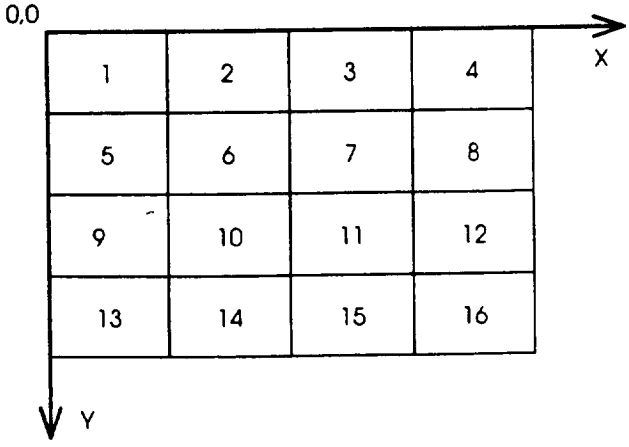

Fig. 2—Coordinate reference for a global image made of 16 contiguous fields of view.

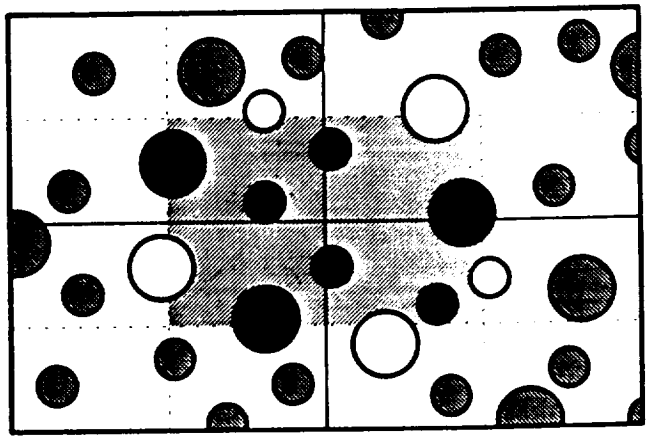

Fig. 4—The measurement frame for image analysis.

of numbers. The particles, which are partly in the measurement frame and whose centroids are outside the measurement frame under consideration (white particles in Figure 4), are accounted for and measured when the corresponding measurement frames containing their respective centroids are analyzed.* In this manner, centroid coordinates and particle size of different particles *are* measured, and they are reported only once. There is a band of exclusion of about 100-pixel width all around the composite global image (consisting of 35 fields of view), which does not belong to any measurement frame (region bounded by broken lines and global frame boundaries in Figure 3), and hence no measurements are performed on the particles whose centroids are in this band. The error due to this "global" edge effect is expected to be very small, and it decreases with the increase in the number of fields of view in the composite global image.

*These particles would be excluded from measurements if the measurements were performed on random disconnected fields of view; this is the edge effect. Due to this edge effect, the microstructural distances involving these particles would not be included in measured distance distributions, resulting in a bias of unknown extent.

The data on the (X, Y) centroid coordinates and the particle section sizes form the input for the computer program used to calculate the K function, radial distribution function, and the nearest-neighbor distribution function pertaining to the 2-D metallographic section on which the measurements have been performed. To calculate the K function, the program proceeds as follows. Let m be the total number of particles on which the measurements are performed, and let (X_1, Y_1), (X_2, Y_2), . . . (X_i, Y_i), . . . (X_m, Y_m) be the centroid coordinates of the particles having the sizes $\tau_1, \tau_2, \ldots \tau_i, \ldots \tau_m$. The program calculates the distances between every particle (X_i, Y_i) and all other $(m\text{-}1)$ particles. It then computes the number of particle centroids at a distance less than r from the particle at (X_i, Y_i), and repeats this calculation for all values of the index i, from 1 to m; the average value of this quantity (properly normalized by magnification) is the estimate of the K function for that value of r. The procedure is repeated for all the desired values of r to obtain the estimate of the function $k(r)$ for the 2-D metallographic section. The program also computes the total number of particle sections per unit area of metallographic plane, N_A. These estimates of $k(r)$ and N_A together with Eq. [4] are then utilized to compute the radial distribution function $g(r)$. The pair correlation function can be also estimated by using a similar procedure. The nearest-neighbor distribution can be estimated simply by recording the distances between the particle centroids and respective nearest particles.

IV. A PRACTICAL EXAMPLE

The electrical conductivity and other physical properties of polymer matrix composites containing hollow spherical carbon particles in a polymeric resin matrix are of interest for certain electrical shielding applications. In such a material, the conductivity of the polymeric matrix is significantly lower than that of the carbon particulate. Thus, the conductivity and other electrical properties of the composite are very sensitive to the spatial arrangement of the carbon particles in the microstructure and the interparticle contacts among these particles. The experimental measurements of the microstructural distance distributions of the hollow carbon particles in the polymer resin matrix have been performed to demonstrate the image analysis procedure developed in Section III. The measurements are performed on this composite because it is easy to fabricate in the laboratory, its electrical properties are sensitive to the microstructural spatial arrangement, and the material is of practical interest for certain aerospace applications.

A. *Material*

The hollow spherical carbon particles were supplied by Carbosphere Inc. (United States). Figure 5 shows the size distribution of these particles. The polymeric resin (araldite) and the hardener were supplied by CIBA GEYGI (France). The resin, the hardener, and the particulate powder were mixed in the appropriate proportions, and the mixture was heated in vacuum to degas the material and to decrease the viscosity of the polymer. It takes about 10 hours for the polymer to harden completely, and hence to minimize the particle segregation due to gravitational effect (the specific gravity of particles is significantly lower than the liquid polymer), the molds were slowly rotated during the hardening of the polymer. The specimens having particulate volume fraction of 0.29 and 0.47 were prepared in this manner.

B. *Materiallography and Image Analysis*

The specimens were cut, mounted, and polished on a series of SiC polishing papers, followed by polishing on diamond cloths using automatic polishing wheels. Figure 6 shows a typical microstructure of the composite observed on a random metallographic plane. The carbon particles are round in shape, and there is a range of particle sizes. In Figure 6, the dark regions are the "hollows" created by the intersections of hollow spherical particles with the sectioning plane. The bright regions

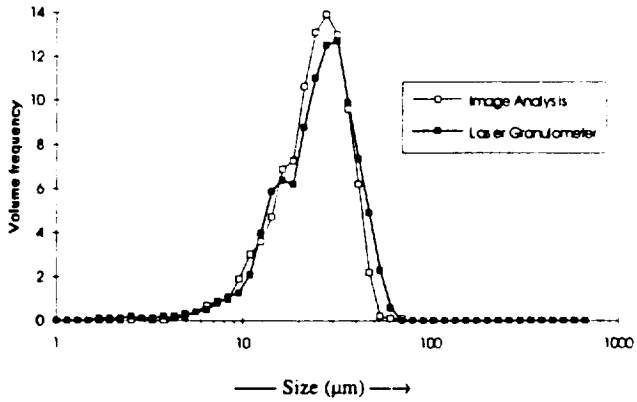

Fig. 5—Frequency distribution of the particles. The volume frequency is the fraction of total particle volume in a given size range. The curves given by image analysis and granulometry are in reasonable agreement with each other.

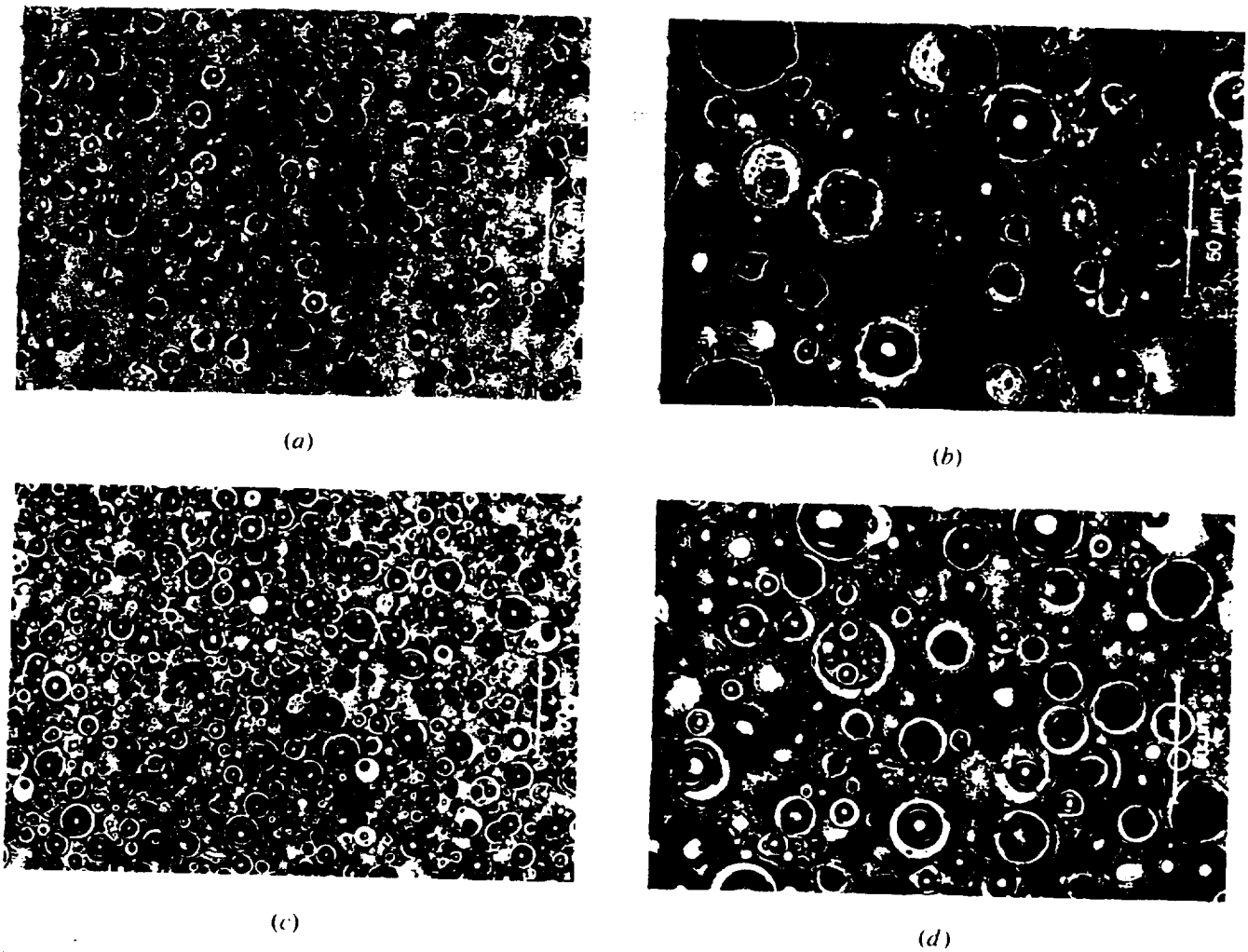

Fig. 6—Microstructures observed in a metallographic section: (*a*) 29 pct particulate volume fraction specimen at magnification 200 times, (*b*) 29 pct particulate volume fraction specimen at magnification 500 times, (*c*) 47 pct particulate volume fraction specimen at magnification 200 times, and (*d*) 47 pct particulate volume fraction specimen at magnification 500 times.

are due to near-tangential intersections between the carbon particle shells and the metallographic plane. The contrast between the particles and the matrix is not good, and hence a number of image transformations are necessary to develop the appropriate contrast *via* image processing.[25,26]

The image analysis and measurements were performed at a microscope magnification of 500 times, yielding a pixel size of 0.325 μm. At this magnification, on the image analyzer screen, the average particle size is about 50 pixels, permitting estimation of particle sizes and interparticle distances with an error of less than 5 pct. In the low volume fraction specimen (29 pct particulate), the measurements were performed on 105 fields of view (at magnification 500 times) spread over three independent composite global image frames (35 fields of view each). In the specimen containing 47 pct carbon particulate, the measurements were performed on 70 fields of view at magnification 500 times spread over two independent composite global image frames, each composed of 35 fields of view. The image analysis procedure was used to obtain the (X, Y) centroid coordinates and the particle section sizes, as described in the last section. The $k(r)$ function, the radial distribution function $g(r)$, and the nearest-neighbor distribution function $p(r)$ were estimated from these data by using a computer program written in the C language. These results are discussed subsequently.

C. *Results and Discussion*

Figure 7 shows the variation of the function $k(r)$ with the microstructural distance r between the particle section centroids observed in a metallographic plane. Recall that $k(r)$ represents an average number of particle section centroids at a distance less than r from an arbitrary particle centroid. The value of $k(r)$ increases monotonically with r, it approaches 0 as r approaches 0, and it tends to infinity as r goes to infinity, as expected. At any given value of r, $k(r)$ is higher for the high volume fraction specimen than for the lower volume fraction specimen. Figure 8 shows the radial distribution function $g(r)$ for the two specimens plotted against the normalized microstructural distance $(r/\bar{r})$, where $\bar{r}$ is the average particle

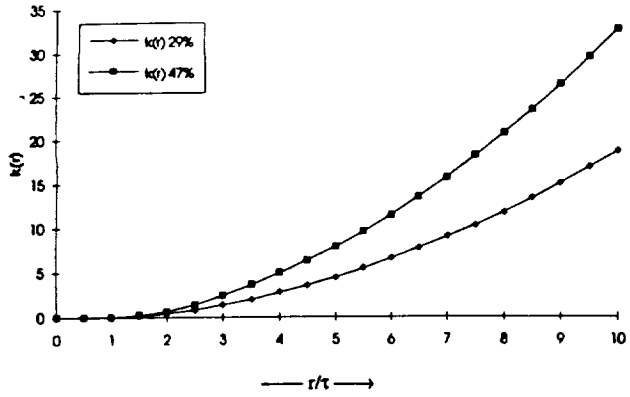

Fig. 7—Estimated K-function of the carbon particle sections observed in a metallographic plane.

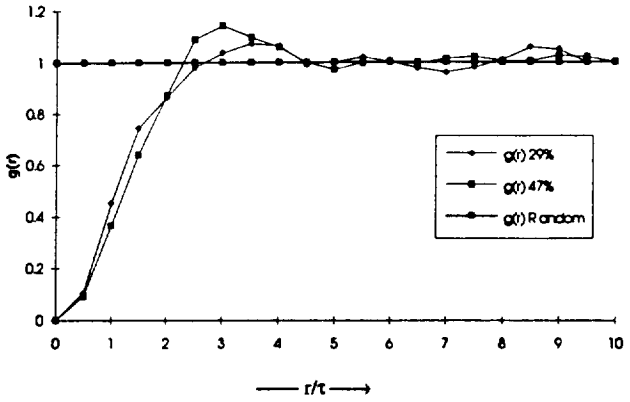

Fig. 8—Estimated radial distribution function of the carbon particle sections observed in a metallographic plane.

section size. The first maximum in the radial distribution function occurs at about $(r/\bar{r})$ equal to 3.0 for the high volume fraction specimen and at $(r/\bar{r})$ equal to 3.5 for the low volume fraction specimen. These distances indicate the maximum likelihood of finding a particle section centroid from any given particle in a metallographic plane. It is important to recognize that the *normalized* radial distribution functions are different for the two specimens having different volume fractions. This is indicative of the intrinsic effect of volume fraction on the spatial arrangement of the particulate. The radial distribution function approaches 1 at distances larger than about five times the average particle section size (although very small perturbations around this mean value exist). Recall that for randomly distributed particle centroids, $g(r)$ is equal to 1. This shows that for the present specimens, particle-particle affinities/repulsions are negligible at distances larger than about five times the average particle size. This information is useful for the computer simulation models. Due to memory limitations, in the computer simulation studies, only a finite extent of microstructural volume can be simulated, and it is of interest to simulate the minimum microstructural volume (called representative volume) that gives the reliable process information. For the processes where only short-range particle-particle interactions are important, the distance beyond which $g(r)$ approaches 1 should provide a realistic measure of the "representative volume element" for computer simulation models.

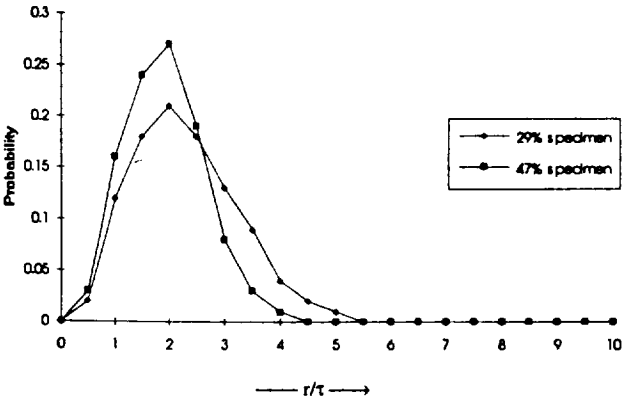

Fig. 9—Estimated nearest-neighbor probability distribution of the distances between carbon particles in the polymer matrix composite.

Figure 9 shows the estimated nearest-neighbor distribution function for the two specimens under investigation, plotted against the normalized nearest-neighbor distance. The average nearest-neighbor distances are 17.0 and 14.6 μm for the specimens having 0.29 and 0.47 particulate volume fraction, respectively.

ACKNOWLEDGMENTS

This research was conducted at Georgia Institute of Technology during LP's assignment as visiting scientist, sponsored by Aerospatiale, France. LP gratefully acknowledges the financial support from Aerospatiale, France. AMG gratefully acknowledges financial support from U.S. National Science Foundation (Grant No. DMR-9301986) and Microgravity Science Applications Division, NASA (Grant No. NAG3-1651) for his contribution to this research.

REFERENCES

1. W.T. Whited, A.M. Gokhale, and N.U. Deshpande: *Microstructural Sci.*, 1994, vol. 21, pp. 107-19.
2. W.T. Whited: M.S. Thesis, Georgia Institute of Technology, Atlanta, GA, 1992.
3. J.R. Brockenbrough, S. Suresh, and H.A. Wienecke: *Acta Metall. Mater.*, 1991, vol. 39, pp. 735-52.
4. B.F. Sorensen and R. Talreja: *Mech. Mater.*, 1993, vol. 16, pp. 351-63.
5. C.W.J. Beenakker: *Phys. Rev. A*, 1986, vol. 33, p. 4482.
6. M. Marder: *Phys. Rev. Lett.*, 1985, vol. 55, p. 2953.
7. R.T. DeHoff: *Acta Metall. Mater.*, 1991, vol. 39, pp. 976-82.
8. R.M. German: *Metall. Trans. A*, 1987, vol. 18A, pp. 909-14.
9. Sung-Chul Yang and R.M. German: *Scripta Metall. Mater.*, 1992, vol. 26, pp. 95-98.
10. E. Nes and J.K. Solberg: *Mater. Sci. Technol.*, 1986, vol. 2, pp. 19-25.
11. Rolf Sandstrom: *Z. Metallkd.*, 1980, vol. 71, pp. 681-88.
12. J.R. Rice and M.A. Johnson: *Inelastic Behavior of Solids*, M.F. Kamninen, ed., McGraw-Hill, New York, NY, 1970.
13. G.T. Hahn and A.R. Rosenfield: *Metall. Trans. A*, 1975, vol. 6A, pp. 653-67.
14. D.S. Wilkinson: *Acta Metall.*, 1988, vol. 36, pp. 2055-63.
15. R. Raj and S. Baik: *Metal. Sci.*, 1980, Aug.–Sept., pp. 385-92.
16. S. Chandrasekhar: *Rev. Mod. Phys.*, 1943, vol. 15, pp. 86-89.

17. A.J. Ardell and P.P. Bansal: *Metallography*, 1972, vol. 5, pp. 97-111.
18. H. Schwartz and H.E. Exner: *J. Microsc.*, 1983, vol. 129, pp. 155-69.
19. K.H. Hanish and D. Stoyan: *J. Microsc.*, 1980, vol. 122, part 2, pp. 131-41.
20. J.A. Given, J. Blawzdziewicz, and G. Stell: *J. Chem. Phys.*, 1990, vol. 93, p. 8156.
21. K.H. Hanish: *Biometrics J.*, 1983, vol. 25, pp. 731-38.
22. B.D. Ripley: *Spatial Statistics*, John Wiley and Sons, London, 1981.
23. K.H. Hanish, D. Konig, and D. Stoyan: *J. Microsc.*, 1985, vol. 140, part 3, pp. 361-70.
24. V. Horelek and J. Klofac: in *MiCon-90: Advances in Video Technology for Microstructural Control*, G.F. Vander Voort, ed., ASTM STP 1094, ASTM, Philadelphia, PA, 1991, pp. 199-213.
25. J.L. Chermant and M. Coster: *Précis d'analyse d'images*, CNRS, Paris, 1985.
26. J. Serra: *Image Analysis and Mathematical Morphology*, Academic Press, London, 1982.